

Lateral Leads Drive Risk Prediction in Brugada Syndrome: A Deep Learning Study

*Original*

Lateral Leads Drive Risk Prediction in Brugada Syndrome: A Deep Learning Study / Randazzo, V., Casella, A., Pasero, E., Giustetto, C., Casu, G., Berne, P., Fancello, T., Gaita, F.. - ELETTRONICO. - (2026). (2026 IEEE Medical Measurements & Applications (MeMeA) Montevideo (Ury) 7-10 April 2026) [10.1109/MeMeA69746.2026.11537375].

*Availability:*

This version is available at: 11583/3011998 since: 2026-06-12T22:24:47Z

*Publisher:*

IEEE

*Published*

DOI:10.1109/MeMeA69746.2026.11537375

*Terms of use:*

This article is made available under terms and conditions as specified in the corresponding bibliographic description in the repository

*Publisher copyright*

IEEE postprint/Author's Accepted Manuscript

©2026 IEEE. Personal use of this material is permitted. Permission from IEEE must be obtained for all other uses, in any current or future media, including reprinting/republishing this material for advertising or promotional purposes, creating new collecting works, for resale or lists, or reuse of any copyrighted component of this work in other works.

(Article begins on next page)

# Lateral Leads Drive Risk Prediction in Brugada Syndrome: A Deep Learning Study

Vincenzo Randazzo  
Politecnico di Torino  
Turin, Italy  
vincenzo.randazzo@polito.it

Alessandro Casella  
Politecnico di Torino  
Turin, Italy  
alessandro.casella@polito.it

Eros Pasero  
Politecnico di Torino  
Turin, Italy  
eros.pasero@polito.it

Carla Giustetto  
Department of Medical Sciences  
University of Turin  
Città della Salute e della Scienza  
Turin, Italy

Gavino Casu  
Department of Cardiology  
University of Sassari  
AOU Sassari  
Sassari, Italy

Paola Berne  
Department of Cardiology  
University of Sassari  
AOU Sassari  
Sassari, Italy

Tatiana Fancello  
Department of Cardiology  
University of Sassari  
AOU Sassari  
Sassari, Italy

Fiorenzo Gaita  
Department of Medical Sciences  
University of Turin  
J Medical  
Turin, Italy

**Abstract**—Sudden cardiac death in Brugada syndrome (BrS) poses a severe stratification dilemma, particularly for asymptomatic individuals with traditional risk markers, such as spontaneous type-1 patterns or family history. While current diagnostic protocols exclusively prioritize the right ventricular outflow tract (RVOT) via right precordial leads, emerging evidence suggests that the arrhythmogenic substrate involves a more widespread cardiomyopathy. To address this limitation, this study presents a deep learning framework based on instance-space multiple instance learning. This framework is designed to predict life-threatening arrhythmic events in Brugada patients using basal 12-lead ECGs. The model was developed and validated on a retrospective cohort of 89 patients collected in the Piedmont Brugada registry, including 37 subjects with documented malignant arrhythmic events. On a hold-out test set, the proposed approach achieved robust prognostic performance with an area under the ROC curve of 0.74; a safety-oriented threshold optimization yielded a negative predictive value of 0.86, minimizing false negatives in screening scenarios. Beyond classification, this study provides a morphological validation of the learned features: explainability analysis using Grad-CAM revealed that the neural network consistently prioritizes lateral leads (aVL, V<sub>5</sub>, V<sub>6</sub>) over the canonical right precordial leads. Quantitative electrophysiological analysis confirmed the biological plausibility of this focus, linking the detected regions to significant conduction abnormalities, including prolonged QRS duration and altered S-wave morphology. These findings indicate that lateral depolarization abnormalities represent a critical, yet overlooked, predictor of arrhythmic risk in BrS.

**Index Terms**—Brugada syndrome, deep learning, ECG, explainable AI, risk stratification, sudden cardiac death.

## I. INTRODUCTION

In patients with structurally normal hearts, up to 20% of sudden cardiac death (SCD) cases are attributed to Brugada syndrome (BrS) [1]. While defined by a type-1 ST-segment elevation in right precordial leads (V<sub>1</sub>–V<sub>3</sub>), the dynamic nature of its clinical phenotype poses significant challenges to diagnosis and risk stratification [2]. Clinical management relies on a prognostic dichotomy. While ICD therapy is mandatory for

cardiac arrest survivors [3], stratifying asymptomatic patients remains challenging due to the limited specificity of traditional markers like family history or spontaneous type-1 patterns [4], [5]. This uncertainty leads to unnecessary implantations or fatal false negatives, exacerbated by the dynamic nature of arrhythmogenic risk [6], [7].

Although diagnosis targets the right ventricular outflow tract (RVOT), the arrhythmogenic substrate often extends to the right ventricular free wall and lateral myocardium [8]. This global instability manifests as depolarization abnormalities in limb leads (prominent S-wave in I, reciprocal R-wave in aVR) and inferolateral leads (fragmented QRS or early repolarization in II, III, aVF, V<sub>5</sub>–V<sub>6</sub>) [9].

To overcome current limitations in prognosis, this study proposes a deep learning (DL) framework for BrS risk stratification that relies on 12-lead ECG recordings. Designed to bridge the gap between artificial intelligence (AI) performance and clinical trust, the architecture is validated through physiological anchors. Morphological analysis via gradient-weighted class activation mapping (Grad-CAM) confirms the network attention extends to lateral leads (V<sub>5</sub>, V<sub>6</sub>, aVL), identifying latent conduction delay markers (see Section IV-B).

## II. BACKGROUND AND RELATED WORKS

In the diagnostic setting of BrS, DL has shown the ability to reveal subtle ECG patterns that escape human visual assessment [10], and recent architectures have specifically targeted borderline presentations, thereby enhancing detection performance [11]. Regarding risk stratification, the key to predicting ventricular arrhythmias (VA) lies strictly within the raw ECG data [12]. Computational models have demonstrated superior prognostic performance compared to conventional clinical scores [13], achieving higher sensitivity in identifying high-risk patients [14]–[16]. Methodological advancements have further refined this predictive capability through the adoption

of vision transformers [17] and the integration of autonomic modulation features [18]. However, the opaque nature of deep neural networks (DNNs) hinders clinical translation. While explainable AI (XAI) techniques are increasingly adopted, current applications are often limited to qualitative inspection without rigorous physiological validation [19]. Table I summarizes the quantitative prognostic performance of recent state-of-the-art AI applications in BrS.

TABLE I  
QUANTITATIVE COMPARISON OF AI PROGNOSTIC MODELS FOR BrS

Study (Year)	Methodology	AUC	Sens.	NPV
Nakamura [15] (2023)	2D CNN	0.80	0.73	0.87
Ishida [16] (2025)	ML (SVM)	0.77	0.60	-
Randazzo [17] (2025)	Vision Transformer	-	0.90	0.95
<b>Proposed (2026)</b>	<b>1D CNN (MIL)</b>	<b>0.74</b>	<b>0.86</b>	<b>0.86</b>

### III. METHODS

#### A. Patient Population and High-Risk Cohort's ECG Selection

The study population (89 patients, 226 ECGs), enrolled from several hospitals in the Piedmont region, Italy [20], was retrospectively partitioned into two distinct cohorts: a high-risk group (*Event*) and a low-risk control group (*Control*). The *Event* cohort comprises  $N = 37$  patients who experienced documented major arrhythmic events, specifically SCD or aborted SCD (aSCD) (59.5%), appropriate ICD shocks (37.8%), or arrhythmic syncope (2.7%). The *Control* cohort includes  $N = 52$  low-risk asymptomatic subjects, predominantly (55.8%) non-inducible at electrophysiological study (EPS) [21]. This study was conducted according to the guidelines of the Declaration of Helsinki, and approved by the Institutional Review Board of Città della Salute e della Scienza Hospital, Turin, Italy (*Protocol code: 248/2017, date of approval: 22 February 2017*). Informed consent was obtained from all subjects involved in the study.

The high-risk population was derived from a baseline of  $N_{pat} = 60$  patients with documented BrS and arrhythmogenic

events, comprising a total of  $N_{ecg} = 220$  recordings acquired prior to any epicardial ablation or antiarrhythmic drug initiation (e.g., Hydroquinidine) [22], [23]. A rigorous multi-step exclusion protocol was applied to ensure data quality and integrity, as illustrated in Fig. 1. Initial filtering at the signal level removed recordings unavailable in raw signal format ( $N_{ecg} = 44$ ). Subsequently, patients with incomplete clinical history were excluded ( $N_{pat} = 13$ ), resulting in the removal of  $N_{ecg} = 26$  associated recordings. To standardize the physiological baseline and minimize confounders, pediatric patients ( $< 15$  years,  $N_{pat} = 3$ ) were discarded. Additionally, patients who never exhibited a Brugada pattern (diagnostic/suspicious type-1) in their ECGs were removed ( $N_{pat} = 4$ ). Finally, to maximize the validity of the model, a temporal filter was applied to the remaining signals: ECGs recorded outside a window of  $\pm 3$  years from the documented event, or those with unknown recording dates, were excluded. This signal-level filtering resulted in the complete exclusion of 3 additional patients who had no remaining valid recordings. The final *Event* cohort thus consisted of  $N_{pat} = 37$  adult patients comprising a total of  $N_{ecg} = 109$  standard 12-lead ECGs.

#### B. Relevant Clinical Characteristics of Patient Population

Table II provides a comprehensive overview of the demographic, genetic, and clinical profiles of the study population. Statistical analysis was performed to ensure correct baseline comparison: continuous variables (mean  $\pm$  SD) were analyzed using unpaired Student's t-test, while categorical data were compared via Chi-square or Fisher's exact test as appropriate.

Demographic analysis indicates a homogeneous population structure. Both cohorts are predominantly male (89.2% vs 82.7%) and well-matched in terms of age (44.2 vs 45.5 years), with no significant differences observed. This male predominance accurately reflects the epidemiology of BrS, which exhibits a significantly higher incidence and risk of life-threatening arrhythmias in men. Consequently, while the

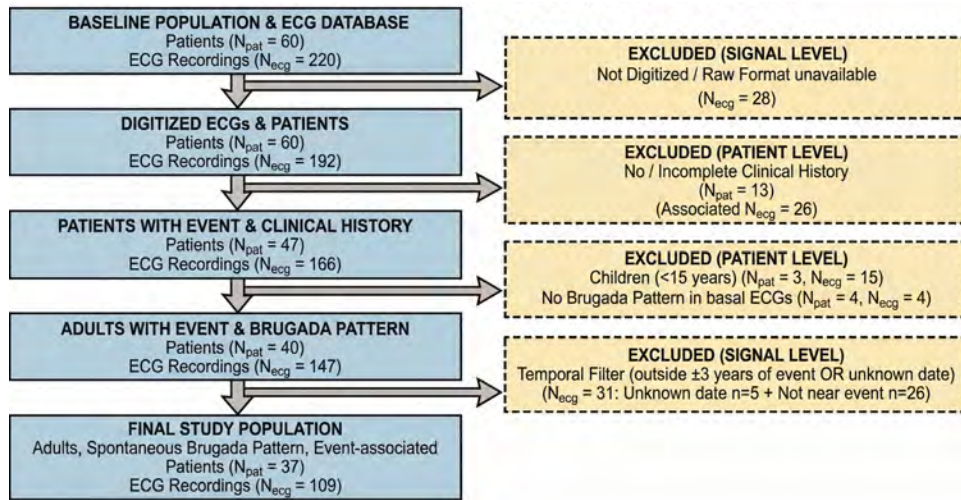


Fig. 1. **Patient and ECG selection flowchart.** The diagram illustrates the stepwise exclusion criteria applied to the baseline population to derive the final study group. ( $N_{pat}$  = Number of Patients;  $N_{ecg}$  = Number of ECG Recordings).

TABLE II  
PATIENT CLINICAL CHARACTERISTICS, OUTCOMES, AND DATASET SIZE

Characteristic / Parameter	Event Group (High Risk)	Control Group (Low Risk)	p-value
<b>Patients (N)</b>	<b>37</b>	<b>52</b>	-
Age (years)	44.2 ± 13.5	45.5 ± 13.9	ns
Male Gender, n (%)	33 (89.2%)	43 (82.7%)	ns
<i>Clinical History &amp; Genetics</i>			
Family History of SCD	9 (24.3%)	6 (11.5%)	ns
Spontaneous type-1 - diagnostic	20 (54.1%)	39 (75.0%)	< 0.05
Spontaneous type-1 - suspicious	17 (45.9%)	13 (25.0%)	< 0.05
SCN5A/SCN1B Mutation	10 (27.0%)	1 (1.9%)	< 0.001
<i>Clinical Phenotype (Event Breakdown)</i>			
SCD / aSCD	22 (59.5%)	-	-
Appropriate ICD Shock	14 (37.8%)	-	-
Arrhythmic Syncope	1 (2.7%)	-	-
<i>EPS</i>			
EPS Performed, n (%)	19 (51.4%)	29 (55.8%)	ns
- Inducible (Positive)	13 (68.4%)*	0 (0%)	< 0.001
- Non-inducible (Negative)	6 (31.6%)*	29 (100%)	
EPS Not Performed, n (%)	18 (48.6%)	23 (44.2%)	ns
<b>Total ECGs (N)</b>	<b>109</b>	<b>117</b>	<b>226 (Total)</b>

\*Percentage relative to the subset of patients who underwent EPS.

limited number of female patients precludes to evaluate potential gender-specific predictive features, the dataset composition ensures that the model is trained on a biologically and clinically representative sample, balanced between the two classes of risk. Consistent with the study design, which aimed to benchmark a strictly low-risk phenotype against the symptomatic cohort, significant differences characterize the clinical and genetic profiles. The significant disparity in SCN5A/SCN1B mutation prevalence (27.0% vs 1.9%) is not an incidental finding but reflects the selection criteria intended to isolate a genetically lower-risk *Control* population.

Furthermore, the distribution of spontaneous ECG patterns reflects a deliberate design strategy intended to challenge the AI model. The *Control* group was intentionally enriched with definite diagnostic type-1 patterns (75.0%) to decouple the classical diagnostic phenotype from the prognostic outcome. Since the type-1 pattern alone lacks specificity for SCD and exhibits significant temporal intermittency—evident here in its lower prevalence among *Event* patients (54.1%)—this composition prevents the network from overfitting on standard  $V_1$ – $V_3$  features. Instead, it encourages the model to look beyond the visible diagnostic criteria, extracting latent arrhythmogenic markers that persist even when the canonical Brugada signature is concealed or ambiguous. Conversely, nearly half of the high-risk patients (45.9%) presented with suspicious type-1 morphologies at baseline.

As detailed in the *Clinical Phenotype* section of Table II, the *Event* group represents a severe condition: 97.3% of patients experienced life-threatening arrhythmias (SCD, aSCD, or appropriate ICD shocks), with only a single case of arrhythmic syncope. Regarding functional stratification, the complete absence of VA inducibility via EPS in tested *Control* subjects confirms the strict safety margins applied during cohort selection, ensuring a reliable ground truth for the low-risk class. Conversely, within the *Event* group, inducibility was significantly higher (68.4%). However, nearly one-third

(31.6%) of these high-risk patients were non-inducible and a further 48.6% did not undergo the EPS. This meaningful proportion of false negatives highlights the inherent limitations of current invasive stratification tools and underscores the necessity for the proposed DL approach to identify substrates missed by standard provocation protocols.

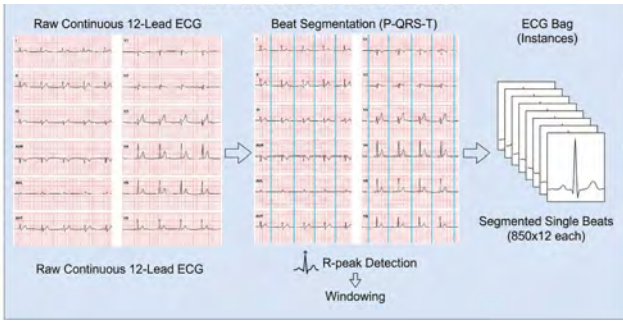
### C. Neural Network Architecture

The overall architecture of the proposed prognostic system is illustrated in Fig. 2. In contrast to common DL strategies that frequently downsample inputs to reduce computational load [24], this framework is specifically designed to preserve high-frequency morphological details, such as fQRS and ventricular late potentials, which are critical markers of slow conduction in BrS. The pipeline operates on full-resolution signals sampled at 1000 Hz and consists of four sequential stages.

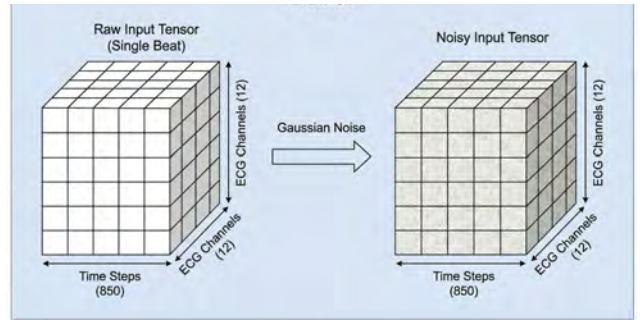
1) *Pre-processing and Augmentation*: The continuous signal undergoes an automated segmentation process based on the methodology established in [25], as depicted in Fig. 2a. By detecting R-peaks, fixed-length temporal windows of 850 ms are extracted centered on each heartbeat, converting the continuous recording into a set of discrete local instances (called *ECG Bag*). Formally, this frames the task as an instance-space multiple instance learning (MIL) problem [26], where the risk label of the *ECG Bag* is propagated to its constituent instances (beats) during training. To improve the model’s generalization capability and robustness against real-world acquisition noise, a data augmentation step is applied (see Fig. 2b). *Gaussian noise* is injected into the raw input tensor ( $850 \times 12$ ), generating a noisy representation that forces the network to learn resilient morphological features rather than overfitting on clean signal patterns.

2) *Feature Extraction and Classification*: The core of the framework is a 1D-convolutional neural network (CNN) that processes each instance within the bag independently (see Fig. 2c). The architecture is designed with alternating blocks of convolution and dimensionality reduction. Specifically, each convolutional layer is followed by *batch normalization* and *ReLU* activation to stabilize learning, while downsampling blocks utilize *max pooling* combined with *dropout* to prevent overfitting. This encoder employs *global average pooling* to condense the temporal features into a compact vector before the final *dense* layer. A *softmax* activation function then outputs a risk probability for each individual heartbeat.

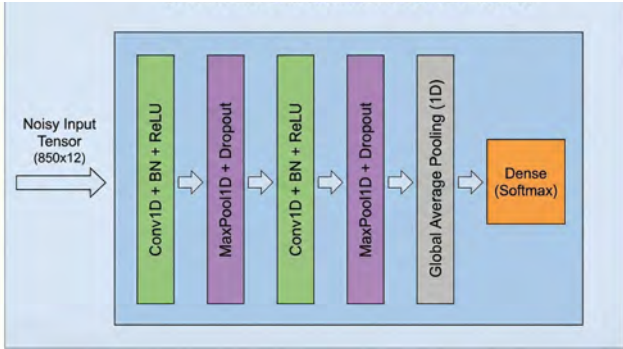
3) *Aggregation and Validation*: Since the risk label is associated with the entire ECG recording rather than the single beat, a post-hoc aggregation mechanism is required (see Fig. 2d). Consistent with the instance-space MIL approach, the individual beat risk scores are fused using a *mean pooling* strategy ( $\sum / N$ ) to derive the final *ECG risk score*. This consensus mechanism ensures that the prediction reflects the pervasive arrhythmogenic substrate across the entire recording. Finally, the black-box decision is subjected to a rigorous validation block (see Fig. 2d). The regions of interest identified via Grad-CAM by the network are cross-referenced with physiological biomarkers quantified through automated signal



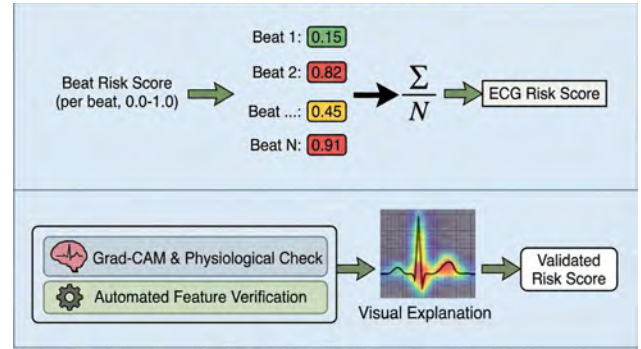
(a) Pre-processing and Segmentation



(b) Input Augmentation



(c) CNN Feature Extractor & Classifier



(d) ECG Scoring & XAI

Fig. 2. **Proposed DL Pipeline.** The framework operates in four stages detailed in the sub-panels: (a) Segmentation of beat-centered windows to form the ECG bag. (b) Injection of Gaussian noise for robustness. (c) Instance-level feature extraction and probability estimation. (d) Aggregation of risk scores via Mean Pooling and interpretability check using Grad-CAM.

processing techniques, ensuring the model’s focus aligns with electrophysiological plausibility.

#### D. Experimental Setup and Data Partitioning

The model was trained for a maximum of 250 epochs with a batch size of 32 instances. The optimization was performed using the Adam optimizer with a learning rate of  $1 \times 10^{-4}$ . The Categorical Cross-Entropy loss function, enhanced with a label smoothing factor of 0.1, improved model generalization and prevent overconfidence. To mitigate overfitting, a dropout rate of 0.25 and an L2 regularization penalty of 0.005 were applied. An early stopping callback was implemented to halt the training process and restore the best weights if the validation loss did not improve for 20 consecutive epochs.

To ensure a robust evaluation of the model’s generalization capabilities and to prevent data leakage, a two-stage partitioning strategy was implemented (see Table III).

First, an independent test set (9 patients, 17 ECGs) was permanently held out. A strict patient-wise criterion was enforced: all recordings belonging to these subjects were isolated before any training process. This subset was used exclusively for

TABLE III  
EXPERIMENTAL DATA PARTITIONING

Subset	Class	Patients	ECGs	% of Total (Patients)
Development Set (5-Fold CV)	Control	47	107	89.9%
	Event	33	102	
Test Set (Hold-out)	Control	5	10	10.1%
	Event	4	7	

the final performance assessment, ensuring that the reported metrics reflect the model’s behavior on biological substrates it has never encountered. The remaining data constituted the development set (80 patients), which was used for model training and hyperparameter optimization. To avoid overfitting to a specific data split, a stratified 5-fold cross-validation (CV) scheme was adopted. In this process, the development set was randomly divided into 5 folds (patient-wise). In each iteration, the model was trained on four folds and validated on the remaining one. This procedure ensures that every non-test patient serves as a validation sample exactly once, providing a statistically reliable estimate of the model’s stability during the development phase.

## IV. RESULTS AND DISCUSSION

### A. Prognostic Performance and Training Dynamics

1) *Training Stability and Phenotypic Anchors:* A retrospective analysis of the CV dynamics revealed that training stability was heavily dependent on the inclusion of specific high-risk subjects, termed *phenotypic anchors*. In validation partitions where these key subjects were excluded from the training set, the model exhibited class collapse, failing to extract discriminative features from the remaining minority class. Conversely, in the optimal training partition where all phenotypic anchors were present, the model successfully escaped local minima (see Table IV).

2) *Threshold Optimization and Test Set Results:* To translate the model’s predictions into a clinically viable screening

tool, the decision threshold was optimized on the calibration set. A weighted Youden index strategy was employed to prioritize specificity, effectively reducing the false positive rate while preserving adequate sensitivity for clinical screening. Table IV presents this final performance: the model achieved an accuracy of 0.71 and an area under the ROC curve (AUC) of 0.74. The weighted optimization strategy resulted in a sensitivity of 0.86 and a specificity of 0.60. This profile represents a favorable clinical trade-off: it maintains a high capability to detect life-threatening substrates, with a negative predictive value (NPV) of 0.86 while offering a significantly higher specificity compared to standard high-sensitivity configurations, thus reducing the rate of unnecessary follow-ups.

TABLE IV  
PERFORMANCE COMPARISON: VALIDATION VS. INDEPENDENT TEST SET

Scenario	Sens	Spec	NPV	PPV	Acc	AUC
Validation (Best Fold)	0.75	0.68	0.88	0.46	0.70	0.71
Test Set (Final)	0.86	0.60	0.86	0.60	0.71	0.74

### B. Morphological Validation via XAI

To ensure that the favorable prognostic performance is driven by physiologically relevant features, a two-tiered explainability analysis was conducted (as detailed in Fig. 2d): a qualitative visual assessment via Grad-CAM and a quantitative validation using standard electrophysiological metrics.

1) *Visual Localization of Arrhythmogenic Substrates*: Fig. 3 presents the saliency map for a representative high-risk subject. The heatmap indicates that the model targets the QRS-ST complex, with high-intensity activation extending beyond the diagnostic right precordial leads ( $V_1$ ,  $V_2$ ) to include lateral (I, aVL,  $V_5$ ) and inferior (II, III) leads. This distributed attention pattern suggests that the risk prediction is driven by widespread conduction delays rather than morphological features localized solely in the RVOT.

2) *Quantitative Physiological Validation*: To corroborate the biological plausibility of the learned features, a quantitative analysis was performed on physiological metrics extracted strictly from correctly classified instances: true positives (TPs) vs. true negatives (TNs). The data presented in Table V reflect this comparison. This beat-wise analysis revealed statistically

significant discrepancies between the discriminative features of high-risk patients and the healthy baseline. Specifically, when the model focused on lateral leads ( $V_5$ , aVL) in the Event group, the QRS duration was significantly prolonged ( $p = 0.004$ ) compared to controls. Moreover, high-attention spots highlighted morphological markers of this delayed activation: leads  $V_6$  and aVL exhibited significantly deeper S-waves ( $p < 0.001$ ) in the high-risk cohort.

TABLE V  
PHYSIOLOGICAL FEATURE COMPARISON: BASELINE (TNs) VS. HIGH-RISK REGIONS (TPs)

Lead	Feature	Control	Event	p-value
$V_5$	QRS Duration (ms)	$97.6 \pm 39.4$	$109.3 \pm 30.0$	0.004
aVL	QRS Duration (ms)	$95.8 \pm 33.2$	$108.2 \pm 27.6$	0.004
$V_6$	S-Wave Ampl. (mV)	$-0.08 \pm 0.08$	$-0.20 \pm 0.05$	$< 0.001$
aVL	S-Wave Ampl. (mV)	$-0.17 \pm 0.08$	$-0.36 \pm 0.14$	$< 0.001$

### V. CONCLUSIONS AND CHALLENGES

This study validates an interpretable DL framework for risk stratification in BrS using an instance space MIL architecture. The model demonstrates robust generalization capabilities, maintaining consistent performance metrics on the independent test set compared to the validation phase (AUC 0.74 vs 0.71), with a notable improvement in sensitivity (see Table IV). These findings challenge the traditional diagnostic paradigm by identifying critical arrhythmogenic substrates in the lateral leads (I, aVL,  $V_5$ ,  $V_6$ ) rather than solely in the right precordial leads (see Fig. 3 and Table V).

The reliance on a brief recording represents a significant constraint compared to continuous 24-hour Holter monitoring, which would allow for the detection of transient anomalies. Since the phenotypic expression of BrS is notoriously intermittent, spatiotemporal fluctuations driven by autonomic modulation or drug intake can temporarily mask ECG features. Therefore, while the aggregate data confirm a warning signal in the pre-event window, this tool acts as a probabilistic assessor of current instability rather than a deterministic oracle of future outcomes.

Finally, it must be acknowledged that the overall quantity of available data is limited relative to standard requirements for training DNNs. However, considering that BrS is a rare

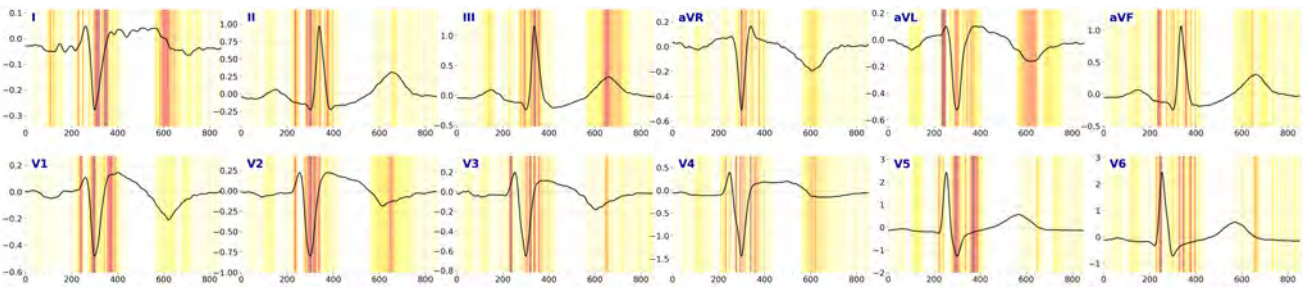


Fig. 3. **Explainability Analysis via Grad-CAM.** Saliency map of a representative High-Risk patient (TP). The heatmap overlay identifies the QRS-ST complex as the primary region of interest. The model’s attention is not confined to the diagnostic right precordial leads but extends strictly to I, II, III, aVL,  $V_5$ , suggesting that the risk prediction is driven by markers of global conduction delay rather than localized RVOT morphological patterns alone. The x-axis represents time in milliseconds (ms), the y-axis indicates the electrical amplitude in millivolts (mV), and the heatmap color intensity reflects the normalized Grad-CAM relevance score.

condition, this single-center cohort represents a highly characterized and valuable clinical sample. To ensure robust training and mitigate the risk of overfitting on this restricted dataset, several strict methodological safeguards were implemented. First, the adoption of the MIL paradigm inherently acted as a data multiplier: rather than learning from 226 static recordings, the model was trained on thousands of individual segmented beats. Second, a lightweight 1D CNN architecture coupled with extensive regularization techniques, including L2 weight decay, dropout, label smoothing, and on-the-fly data augmentation was employed. Finally, a rigorous patient-wise stratified splitting strategy was enforced to guarantee zero data leakage across the training, validation, and independent test sets. Beyond the general sample size, the specific scarcity of raw digital ECGs for patients with arrhythmic syncope (see Table II) restricted the study to the most severe phenotypes (SCD, aSCD, and ICD shock). Consequently, future efforts will prioritize the collection of larger multicenter datasets to enhance model generalization and will integrate the syncope subgroup as digital data become available.

## REFERENCES

- [1] S. G. Priori, C. Blomström-Lundqvist, A. Mazzanti, N. Blom, M. Borggrefe, J. Camm, P. M. Elliott, D. Fitzsimons, R. Hatala, G. Hindricks, *et al.*, “2015 esc guidelines for the management of patients with ventricular arrhythmias and the prevention of sudden cardiac death,” *Europace*, vol. 17, no. 11, pp. 1601–1687, 2015.
- [2] L. Barca, G. Mascia, M. Haissaguerre, C. Monaco, H. Xhakupi, L. Carmisciano, A. Saglietto, C. Giustetto, P. Di Donna, E. Arbelo, *et al.*, “Incidence of spontaneous brugada ecg during follow-up in patients with drug-inducible pattern: A systematic review and meta-analysis,” *Heart Rhythm*, 2025.
- [3] V. Probst, C. Veltmann, L. Eckardt, P. Meregalli, F. Gaita, H. Tan, D. Babuty, F. Sacher, C. Giustetto, E. Schulze-Bahr, *et al.*, “Long-term prognosis of patients diagnosed with brugada syndrome: results from the finger brugada syndrome registry,” *Circulation*, vol. 121, no. 5, pp. 635–643, 2010.
- [4] F. Gaita, N. Cerrato, C. Giustetto, A. Martino, L. Bergamasco, M. Millesimo, L. Barbonaglia, P. Carvalho, D. Caponi, A. Saglietto, *et al.*, “Asymptomatic patients with brugada ecg pattern: long-term prognosis from a large prospective study,” *Circulation*, vol. 148, no. 20, pp. 1543–1555, 2023.
- [5] C. Giustetto, G. Nangeroni, N. Cerrato, B. Rudic, E. Tüllümen, E. Gribaudo, D. F. Giachino, L. Barbonaglia, L. M. Biava, P. Carvalho, *et al.*, “Ventricular conduction delay as marker of risk in brugada syndrome. results from the analysis of clinical and electrocardiographic features of a large cohort of patients,” *International Journal of Cardiology*, vol. 302, pp. 171–177, 2020.
- [6] C. Giustetto, N. Cerrato, V. Dusi, F. Angelini, G. De Ferrari, and F. Gaita, “The brugada syndrome: pharmacological therapy,” *European Heart Journal Supplements*, vol. 25, pp. C32–C37, 2023.
- [7] P. Berne, F. Usai, E. Silva, I. Melis, T. Fancello, A. Onida, P. Merella, F. Figus, J. Brugada, and G. Casu, “Diagnosis of brugada syndrome affects quality of life and psychological status,” *Frontiers in Cardiovascular Medicine*, vol. 11, p. 1429814, 2024.
- [8] M. Pieroni, P. Notarstefano, A. Oliva, O. Campuzano, P. Santangeli, M. Coll, M. Nesti, A. Carnevali, A. Fraticelli, A. Iglesias, *et al.*, “Electroanatomic and pathologic right ventricular outflow tract abnormalities in patients with brugada syndrome,” *Journal of the American College of Cardiology*, vol. 72, no. 22, pp. 2747–2757, 2018.
- [9] S. Georgopoulos, K. P. Letsas, T. Liu, M. Kalafateli, P. Korantzopoulos, G. Bürkle, K. Vlachos, G. Giannopoulos, M. Efremidis, S. Deftereos, *et al.*, “A meta-analysis on the prognostic significance of inferolateral early repolarization pattern in brugada syndrome,” *EP Europace*, vol. 20, no. 1, pp. 134–139, 2018.
- [10] L. Melo, G. Ciconte, A. Christy, G. Vicedomini, L. Anastasia, C. Pappone, and E. Grant, “Deep learning unmasks the ecg signature of brugada syndrome,” *PNAS nexus*, vol. 2, no. 11, p. pgad327, 2023.
- [11] V. Randazzo, A. Casella, S. Caligari, F. Gaita, C. Giustetto, and E. Pasero, “A three-class ai model for brugada syndrome detection to improve diagnostic accuracy in ecg analysis,” in *2025 IEEE Medical Measurements & Applications (MeMeA)*, pp. 1–6, IEEE, 2025.
- [12] A. Delinière, A. Baranchuk, J. Gai, F. Bessiere, D. Maucort-Boulch, P. Defaye, E. Marijon, O. Le Vavasseur, D. Dobreanu, A. Scridon, *et al.*, “Prediction of ventricular arrhythmias in patients with a spontaneous brugada type 1 pattern: the key is in the electrocardiogram,” *EP Europace*, vol. 21, no. 9, pp. 1400–1409, 2019.
- [13] J. Sieira, G. Ciconte, G. Conte, C. de Asmundis, G.-B. Chierchia, G. Baltogiannis, G. Di Giovanni, Y. Saitoh, R. Casado-Arroyo, J. Juliá, *et al.*, “Long-term prognosis of drug-induced brugada syndrome,” *Heart Rhythm*, vol. 14, no. 10, pp. 1427–1433, 2017.
- [14] C. J. Leong, S. Sharma, J. Seth, and S. W. Rabkin, “Artificial intelligence streamlines diagnosis and assessment of prognosis in brugada syndrome: a systematic review and meta-analysis,” *Connect Health Telemed*, vol. 3, 2024.
- [15] T. Nakamura, T. Aiba, W. Shimizu, T. Furukawa, and T. Sasano, “Prediction of the presence of ventricular fibrillation from a brugada electrocardiogram using artificial intelligence,” *Circulation Journal*, vol. 87, no. 7, pp. 1007–1014, 2023.
- [16] S. Ishida, M. Furutani, M. Nakashima, N. Ishibashi, J. Maeda, T. Sakai, N. Oguri, S. Miyamoto, S. Miyauchi, S. Okamura, *et al.*, “Risk stratification of major arrhythmia events in japanese patients with brugada syndrome using machine learning models,” *Heart Rhythm O2*, vol. 6, no. 7, pp. 987–994, 2025.
- [17] V. Randazzo, S. Caligari, E. Pasero, C. Giustetto, A. Saglietto, W. Bertarello, A. Averbuch, M. Marcus-Kalish, V. Zheludev, and F. Gaita, “A vision transformer model for the prediction of fatal arrhythmic events in patients with brugada syndrome,” *Sensors*, vol. 25, no. 3, p. 824, 2025.
- [18] M. Calvo, V. Le Rolle, D. Romero, N. Behar, P. Gomis, P. Mabo, and A. I. Hernández, “Recursive model identification for the analysis of the autonomic response to exercise testing in brugada syndrome,” *Artificial intelligence in medicine*, vol. 97, pp. 98–104, 2019.
- [19] K. Y. Kan, A. Van Wyk, T. Paterson, N. Ninan, P. Lysyganicz, I. Tyagi, R. Bhasi Lizi, F. Boukrif, M. Alfaifi, A. Mishra, *et al.*, “Beyond the type 1 pattern: comprehensive risk stratification in brugada syndrome,” *Journal of Interventional Cardiac Electrophysiology*, vol. 68, no. 8, pp. 1771–1790, 2025.
- [20] F. Gaita, N. Cerrato, A. Saglietto, and *et al.*, “Long-term risk of arrhythmic events in brugada syndrome: insights from the piedmont brugada registry,” *European Heart Journal Supplements*, vol. 25, pp. C27–C31, 2023.
- [21] C. Giustetto, N. Cerrato, E. Ruffino, E. Gribaudo, C. Scrocco, L. Barbonaglia, F. Bianchi, M. Bortnik, G. Rossetti, P. Carvalho, *et al.*, “Etiological diagnosis, prognostic significance and role of electrophysiological study in patients with brugada ecg and syncope,” *International Journal of Cardiology*, vol. 241, pp. 188–193, 2017.
- [22] J. Brugada, C. Pappone, A. Berruero, G. Vicedomini, F. Manguso, G. Ciconte, L. Giannelli, and V. Santinelli, “Brugada syndrome phenotype elimination by epicardial substrate ablation,” *Circulation: Arrhythmia and Electrophysiology*, vol. 8, no. 6, pp. 1373–1381, 2015.
- [23] A. Andorin, J.-B. Gourraud, J. Mansourati, S. Fouchard, H. Le Marec, P. Maury, P. Mabo, J.-S. Hermida, J.-C. Deharo, B. Delasalle, *et al.*, “The quidam study: hydroquinidine therapy for the management of brugada syndrome patients at high arrhythmic risk,” *Heart Rhythm*, vol. 14, no. 8, pp. 1147–1154, 2017.
- [24] A. M. Alqudah and Z. Moussavi, “A review of deep learning for biomedical signals: Current applications, advancements, future prospects, interpretation, and challenges,” *Computers, Materials & Continua*, vol. 83, no. 3, 2025.
- [25] F. Delrio, V. De Vitis, S. Caligari, V. Randazzo, G. Cirrincione, and E. Pasero, “Enhancing ecg analysis with a hybrid deep learning approach: Automatic detection of significant features,” in *Advanced Neural Artificial Intelligence: Theories and Applications*, pp. 23–33, Springer, 2025.
- [26] H. Han, C. Lian, Z. Zeng, B. Xu, J. Zang, and C. Xue, “Multimodal multi-instance learning for long-term ecg classification,” *Knowledge-Based Systems*, vol. 270, p. 110555, 2023.